Anomalous Higgs Couplings at an $e\,\gamma$ Collider

Debajyoti Choudhury

Department of Physics and Astrophysics,

University of Delhi, Delhi-110007, India.

and

Mamta

Department of Physics,

S.G.T.B. Khalsa College,

University of Delhi, Delhi-110007, India.

Abstract

We examine the sensitivity of $e\,\gamma$ colliders (based on $e^+\,e^-$ linear colliders of c.m. energy 500 GeV) to the anomalous couplings of the Higgs to W-boson via the process $e^-\,\gamma \longrightarrow \nu\,W\,H$. This has the advantage over $e^+\,e^-$ collider in being able to dissociate WWH vertex from ZZH. We are able to construct several dynamical variables which may be used to constrain the various couplings in the WWH vertex.

1 Introduction

The Standard Model (SM) of particle physics, based on the gauged symmetry group $SU(3)_C \times SU(2)_L \times U(1)_Y$, has proven to be incredibly successful in describing the electromagnetic, weak and strong interactions. However, the precise mechanism of the electroweak symmetry breaking and mass generation still remains one of the important open questions of the theory. Within the SM, the breaking of symmetry is realized *via* the Higgs mechanism in which a scalar SU(2) doublet, the Higgs boson (which is not yet an experimental reality) is introduced *ad hoc* and the symmetry spontaneously broken by virtue of the Higgs field acquiring a vacuum expectation value. However, in this realization, the theory suffers from the "naturalness" problem since the running Higgs mass is quadratically divergent necessitating a fine tuning in order to keep the theory perturbative. Conversely, this implies the existence of a cut-off scale Λ (widely believed to be of the order of TeV) above which new physics must appear.

Probing the mechanism of EWSB and the search for a Higgs boson together constitute one of the main goals of present and future TeV-scale colliders. The direct search for the Higgs boson in the CERN LEP experiments sets a lower bound on its mass of $m_H > 114.4$ GeV [1]. The precision electroweak data, on the other hand, favor a light Higgs boson with a mass $m_H \leq 186$ GeV at 95% CL [2]. It should be noted though that both these bounds are model-dependent and, in theories going beyond the SM, maybe modified to a significant degree. For example, in two-Higgs doublet models, with [3] or without supersymmetry [4], the lower limit from direct searches at LEP and elsewhere is still as low as 10 GeV [5]. Similarly, the upper bound on the mass of the (lightest) Higgs in some extensions may be substantially higher [6]. The Large Hadron Collider (LHC) is expected to be capable [7] of searching for the Higgs boson in the entire mass range allowed.

In case a Higgs boson is found at TeV-scale colliders, it is of fundamental importance to check if the Higgs boson is SM-like by studying its couplings to the SM particles. In particular, if no new light particles other than the Higgs boson are detected in the next generation collider experiments, it is even more pressing to determine the Higgs boson couplings as accurately as possible to look for hints for new physics beyond the SM.

As the dominant neutral Higgs production modes at a linear collider proceed via its coupling with a pair of gauge bosons ($VV,\ V = W, Z$), these are expected to be sensitive to the VVH couplings, and departures from their SM values can be probed via such production processes. Kinematical distributions for the process $e^+e^- \to f\bar{f}H$, proceeding via vector boson fusion and Higgsstrahlung have been studied both without [8, 9] and with beam polarization [10, 9]. Anomalous ZZH couplings, expressed in terms of higher dimensional operators, have been studied in Refs.[11, 12, 13, 14, 15] for the LC and in Refs.[16, 17, 18] for the LHC. And whereas Ref. [19] probes the anomalous ZZH and γZH couplings using the optimal observable technique [20], Refs. [9, 21], on the other hand, use asymmetries in kinematical distributions. In Ref. [22], the VVH vertex is studied in the process of $\gamma\gamma \to H \to W^+W^-/ZZ$ using angular distributions of the decay products.

While the aforementioned studies have well established the high resolving power of the e^+e^- linear collider in resolving the ZZH vertex, the sensitivity to the WWH vertex is not as good. As Ref.[9] explicitly exhibits, observables depending on the latter most often also receive contributions from the former (ZZH), thereby making it very difficult to untangle the two. Furthermore, the leading order process at an e^+e^- collider sensitive

to the WWH vertex, namely the $\bar{\nu}_e\nu_e H$ production channel, has too few observables associated with it. It is thus contingent upon us to look for alternative channels with enhanced sensitivity to this vertex.

A high energy $e\ e$ linear collider provides just such a theater in the form of a high energy photon beam option. As the electron (positron) bunches in these colliders are used only once, it is possible to convert electrons to real high-energy photons using the Compton back-scattering of laser light and thus obtain $\gamma\ \gamma$ and $e\,\gamma$ colliders with real photons. With the luminosity and energy of such colliders being comparable to those of the basic $e\ e$ collider [24], one may now consider a process such as

$$e^- + \gamma \to \nu_e + W^- + H\ . \tag{1}$$

Clearly, this process is sensitive to the WWH vertex, but not to the ZZH one. Furthermore, with both the Higgs and the W being visible (in their decay modes), one is offered a plethora of kinematical variables in the construction of suitable observables. Thus, this process suffers from neither of the two aforementioned problems that plagued the dominating channel at the parent e^+e^- machine.

The outline of the paper is as follows: In section 2, we discuss the possible sources and symmetries of various VVH couplings and the rate of the process used to constrain these couplings. A realistic experiment and the acceptance cuts are discussed in section 3. In section 4.1, we construct several observables to constrain the WWH vertex using unpolarized beams at c.m. energies of 500 GeV. The effect of polarized beams is discussed in section 4.2. In section 5, we use the conjugate process ($e^+\ \gamma \longrightarrow \bar{\nu}\ W\ H$) to improve the limits.

2 VVH Couplings

Within the SM as well as its minimal supersymmetric counterpart (MSSM), the only (renormalisable) interaction term involving the Higgs boson and a pair of gauge bosons is the one arising from the Higgs kinetic term. However, once we accept the SM to be only an effective low energy description of some other theory, higher dimensional (and hence non renormalisable) terms are also allowed.

Demanding only Lorentz invariance and gauge invariance, the most general coupling structure may be expressed as

$$\Gamma^V_{\mu\nu} = g_V \left[a_V g_{\mu\nu} + \frac{b_V}{m_V^2}\left(k_{2\mu}k_{1\nu} - g_{\mu\nu}k_1\cdot k_2\right) + \frac{\beta_V}{m_V^2}\epsilon_{\mu\nu\alpha\beta}k_1^\alpha k_2^\beta \right] \tag{2}$$

where k_1^μ and k_2^ν are the momenta of two W's (or Z's) with

$$\begin{aligned} g_W^{SM} &= e\ \cot\theta_W\ M_Z \\ g_Z^{SM} &= 2\ e\ M_Z/\sin 2\theta_W . \end{aligned} \tag{3}$$

In the context of the SM, at the tree level, $a_W^{SM} = a_Z^{SM} = 1$, while the other couplings vanish identically. At the one-loop level or in a different theory, effective or otherwise, these may assume significantly different values.

Trans.	a_W	$\mathcal{R}(b_W)$	$\mathcal{R}(\beta_W)$	$\mathcal{I}(b_W)$	$\mathcal{I}(\beta_W)$
C	$+$	$+$	$+$	$+$	$+$
P	$+$	$+$	$-$	$+$	$-$
$\hat{T}$	$+$	$+$	$-$	$-$	$+$

Table 1: *Transformation properties of the terms in the Lagrangian corresponding to the various couplings.*

In general, each of these couplings can be complex, reflecting possible absorptive parts of the loops, either from the SM or from some new high scale physics beyond the SM. Note, though, that in most processes of interest wherein the amplitude is linear and homogenous in the VVH couplings (*i.e.*, when the Yukawa couplings may be neglected), an overall phase of the couplings is irrelevant. Thus, one phase may be rotated away and we make this choice for a_W, while keeping the rest complex.

A generic multi-doublet model, whether supersymmetric [25] or otherwise [26], is characterized by a sum rule for the couplings of the neutral Higgs bosons to a pair of gauge bosons, namely $\sum_i a^2_{VVH_i} = 1$. Although a_{VVH_i} for a given Higgs boson can be significantly smaller than the SM value (as, for example, may happen in the MSSM), any violation of the above sum rule would indicate either the presence of higher $SU(2)_L$ multiplets or more complicated symmetry breaking structures (such as those within higher-dimensional theories) [26]. On the other hand, such couplings may appear either from higher order corrections to the vertex in a renormalisable theory [27] or from higher dimensional operators in an effective theory [28]. The couplings b_V and β_V can arise from the terms such as $F_{\mu\nu}F^{\mu\nu}\Phi^\dagger\Phi$ or $F_{\mu\nu}\tilde{F}^{\mu\nu}\Phi^\dagger\Phi$ where Φ is the usual Higgs doublet, $F_{\mu\nu}$ is the field strength tensor and $\tilde{F}_{\mu\nu}$ its dual [28]. The effects of still higher dimensional terms in the trilinear vertices of interest can be absorbed into b_V or β_V by ascribing them with non-trivial momentum dependences. Clearly if the cut-off scale Λ of this theory is much larger than the typical energy at which the scattering experiment is to be performed, the said dependence would be weak. Thus, the momentum dependence of the form factors have a rather minor role to play at the first generation linear colliders, especially for $\Lambda \sim 1$ TeV.

Finally, note that, unlike in the case of the ZZH couplings, the various terms in the WWH effective vertex can be ascribed definite properties (see Table 1) under each of the discrete transformations C, P and $\hat{T}$ where $\hat{T}$ stands for the pseudo-time reversal transformation, one which reverses particle momenta and spins but does not interchange initial and final states. That the imaginary parts of b_W and β_W may lead to $CP\hat{T}$-odd observable is, of course, to be expected.

2.1 The process and cross sections

To the lowest order, Higgs production at an $e\gamma$ collider— the process of Equation 1— receives contributions from the three Feynman diagrams shown in Fig.1. In calculating the cross section, we retain contributions only upto the lowest non-trivial order in the anomalous couplings, keeping in view the higher dimensional nature of their origin. Thus

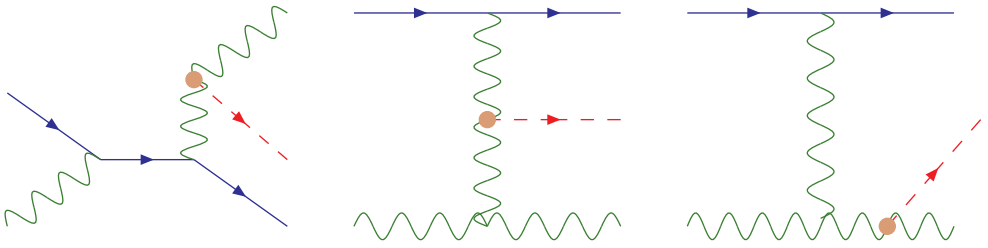

Figure 1: *Feynman Diagrams for* $e^-\gamma \to \nu_e W^- H$.

the cross-section may be written as

$$\sigma = (1 + 2\,\Delta a_W)\sigma_0 + \mathcal{R}(b_W)\sigma_1 + \mathcal{R}(\beta_W)\sigma_2 + \mathcal{I}(b_W)\sigma_3 + \mathcal{I}(\beta_W)\sigma_4. \tag{4}$$

Note that, as in Ref. [9], we have assumed that we are dealing with a SM-like Higgs and hence

$$a_W \equiv 1 + \Delta a_W \tag{5}$$

is close to its SM value.

Being odd under $\hat{T}$, some of the terms in Equation (2) would not contribute, at the linear order, to the total rate, which is a $\hat{T}$ even observable. Thus, to see their effect, we need to restrict ourselves to an appropriate part of the phase space. To this end, consider a frame wherein the initial state e^- points along the positive z-axis and defines, along with the Higgs momentum, the $x - z$ plane. An appropriate phase space choice is described by a restriction of the W to be produced either in the hemisphere above or below this $x - z$ plane, or, in other words, restricting $\sin\phi_{HW}$ (ϕ_{HW} being the azimuthal separation between the Higgs and the W) to either a positive or a negative value. With this constraint applied, the different contributions to the total rate, as a function of the center-of-mass energy is displayed in Fig.2. [Note that a non-zero Δa_W would only rescale the SM rates.]

Clearly, the SM cross-section grows with $\sqrt{s}_{e\gamma}$ for the range shown, a consequence of the presence of the "t"- and "u"-channel diagrams. It can be checked easily that, for each polarization state, the contributions corresponding to $\mathcal{R}(b_W)$, $\mathcal{R}(\beta_W)$ and $\mathcal{I}(\beta_W)$ asymptotically grow faster than the SM cross section σ_0. This is but a reflection of the higher-dimensional nature of the couplings. The contribution proportional to $\mathcal{I}(b_W)$, namely σ_3, on the other hand, grows slower than σ_0. While this may seem surprising at first, this owes itself to the fact that we are considering only the interference terms with the SM and that these typically suffer from at least the same suppressions as the SM piece (this is quite akin to the case of Ref.[9]). In addition, it should be remembered that the unrestricted (*i.e.*, summed over the full phase space) σ_2 and σ_3 vanish identically.

The preceding discussion also indicates that a larger $\sqrt{s_{e\gamma}}$ would increase the sensitivity to almost all the couplings, bar $\mathcal{I}(b_W)$. However, rather than investigate the advantage of varying the center of mass energy, we shall, henceforth, restrict ourselves to a realistic first generation photon collider and emphasize the importance of imposing various kinematic restrictions. Such a choice would naturally restrict us to momentum transfers far below

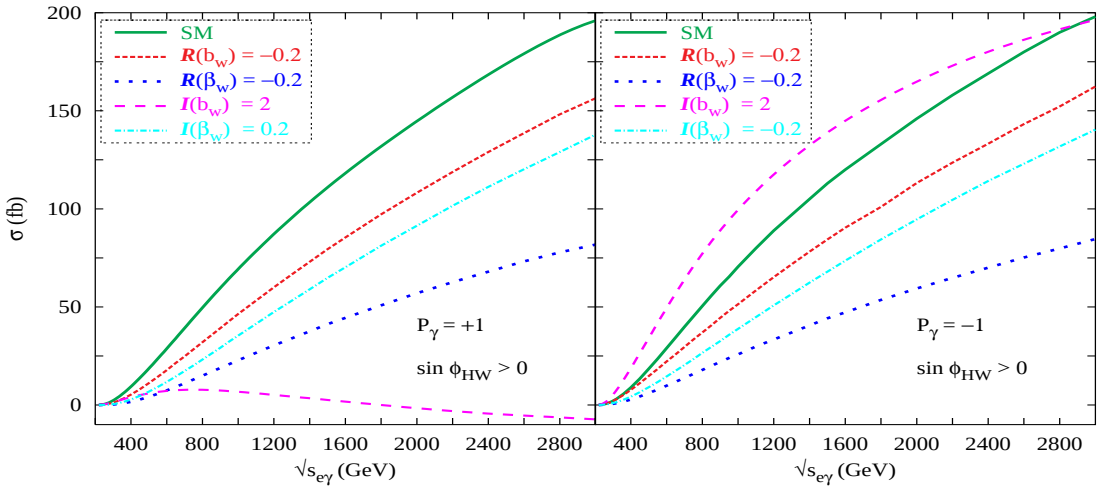

Figure 2: *Partial cross-sections σ_i for $e^-\gamma \to \nu_e W^- H$, with the restriction that* $\sin\phi_{HW} > 0$ *as functions of the c.m. energy for a Higgs boson of mass 120 GeV and particular values for the anomalous couplings. Fully polarized but monoenergetic photons have been used, with the left(right) panels corresponding to $P_\gamma = +1\,(-1)$ respectively. The electron is assumed to be unpolarized.*

the deemed scale of new physics, viz. $\Lambda \sim 1$ TeV, thereby allowing us to neglect any form-factor behavior for these couplings.

A further point to be noted is the large dependence of the $\mathcal{I}(\beta_W)$ and $\mathcal{I}(b_W)$ contributions on the photon polarization, whereas the others have only a minor dependence. This, of course, implies that polarized scattering may be used effectively to isolate the first two, a possibility that we shall return to later.

3 A Realistic Collider Experiment

3.1 The photon collider

Although we have considered a monoenergetic photon beam in deriving the results in the last section, in reality, a high energy monochromatic beam is not possible. Rather, a high energy photon beam is to be obtained by back-scattering a laser beam from an electron/positron beam. The reflected photon beam carries off only a fraction (y) of the $e^\pm$ energy with

$$\begin{aligned} y_{\max} &= \frac{z}{1+z} \\ z &\equiv \frac{4E_bE_L}{m_e^2}\,\cos^2\frac{\theta_{bL}}{2}\,, \end{aligned} \tag{6}$$

where $E_{b(L)}$ are the energies of the incident electron (or positron) beam and the laser respectively and θ_{bL} is the incidence angle. In principle, one can increase the photon energy by increasing the energy of the laser beam. However, a large E_L (or, equivalently, a large z) also enhances the probability of electron positron pair creation through laser and scattered-photon interactions, and consequently results in beam degradation. An optimal choice is $z = 2(1+\sqrt{2})$, and this is the value that we adopt in our analysis.

The cross-sections for a realistic electron-photon collider can then be obtained by convoluting the fixed-energy cross-sections $\hat{\sigma}(\hat{s}, P_\gamma, P_{e^-})$ with the appropriate photon spectrum:

$$\sigma(s) = \int \mathrm{d}y\ \mathrm{d}\hat{s}\ \frac{\mathrm{d}n}{\mathrm{d}y}(P_b, P_L)\ \hat{\sigma}(\hat{s}, P_\gamma, P_{e^-})\ \delta(\hat{s} - ys)\ , \tag{7}$$

where the photon polarization is itself a function of $P_{b,L}$ and the momentum fraction, viz. $P_\gamma = P_\gamma(y, P_b, P_L)$. For simplicity, we shall consider only circularly polarized lasers scattering off polarized electron (positron) beams. The corresponding number-density $n(y)$ and average helicity for the scattered photons are then given by [24]

$$\begin{aligned} \frac{dn}{dy} &= \frac{2\pi\alpha^2}{m_e^2 z \sigma_C} C(y) \\ P_\gamma(y) &= \frac{1}{C(y)}\left[P_b\left\{\frac{y}{1-y} + y(2r-1)^2\right\} - P_L(2r-1)\left(1 - y + \frac{1}{1-y}\right)\right] \\ C(y) &\equiv \frac{y}{1-y} + (1-y) - 4r(1-r) - 2P_bP_Lrz(2r-1)(2-y)\ , \end{aligned} \tag{8}$$

where $r \equiv y/z/(1-y)$ and the total Compton cross-section σ_C provides the normalization.

3.2 The final state

To be quantitative, we shall choose to work with a Higgs boson of mass 120 GeV and a parent e^+e^- machine operating at a center of mass energy of 500 GeV, or, in other words a maximum $\sqrt{s}_{e\gamma}$ of ~ 455 GeV. For such a Higgs mass, the dominant decay channel is the one into a $b\bar{b}$ pair, with the corresponding branching fraction ~ 0.9. And as we want the W momentum to be reconstructible, we restrict ourselves to the $W \longrightarrow q\bar{q}$ mode with a branching fraction ~ 0.68. The final state thus comprises of four jets and missing momentum. Of the jets, two must be b-like and these must reconstruct to m_H and the other two must reconstruct to m_W.

To be detectable, each of the jets must have a minimum energy and they must not be too forward or backward. Furthermore, any two jets should be well separated so as to be recognizable as separate ones. And finally, the events must be characterized by a minimum missing transverse momentum. To be quantitative, our acceptance cuts constitute

$$\begin{aligned} p_T^{\rm miss} &\geq 20\,\mathrm{GeV} & \\ -3.0 \leq \eta_j &\leq 3.0 & \text{for rapidity of each jet} \\ p_T &\geq 10\,\mathrm{GeV} & \text{for each jet} \\ \Delta R_{j_1 j_2} &\geq 0.7 & \text{for each pair of jets} \end{aligned} \tag{9}$$

where $(\Delta R_{j_1 j_2})^2 \equiv (\Delta\phi)^2 + (\Delta\eta)^2$ with $\Delta\phi$ and $\Delta\eta$ denoting the separation between the two jets in azimuthal angle and rapidity respectively.

With only the acceptance cuts in place, and with the use of unpolarized beams (electron, laser as well the beam reflected off), the cross section is

$$\sigma = [4.15\,(1 + 2\,\Delta a_W) - 16.09\,\mathcal{R}(b_W) - 1.96\,\mathcal{I}(\beta_W)]\ \text{fb}\ . \tag{10}$$

As expected, $\mathcal{I}(b_W)$ and $\mathcal{R}(\beta_W)$ do not contribute to the total rate, while $\mathcal{I}(\beta_W)$ makes only a small contribution.

For any such measurement, one may define a statistical measure of agreement with the SM expectations by defining a fluctuation through

$$(\delta\sigma)^2 = \frac{\sigma_{_{SM}}}{\mathcal{L} + \epsilon^2\, \sigma_{_{SM}}^2}. \tag{11}$$

Here $\sigma_{_{SM}}$ is the SM value of the cross-section, $\mathcal{L}$ is the integrated luminosity of the machine and ϵ is the fractional systematic error. We shall, henceforth, consider $\epsilon = 0.01$. Using the total cross sections —Equation 10 —alone, we can then constrain a particular linear combination of couplings, *viz.*

$$\mid 2\, \Delta a_W - 3.88\, \mathcal{R}(b_W) - 0.47\, \mathcal{I}(\beta_W) \mid \leq\ 0.072\ . \tag{12}$$

at the 3σ level.

As can be well appreciated, total cross sections are unlikely to be the most sensitive of probes. For one, this observable is not at all sensitive to either of $\mathcal{I}(b_W)$ and $\mathcal{R}(\beta_W)$. Secondly, it is quite conceivable that contributions proportional to different anomalous pieces have distinct phase space distributions, thereby affording us the possibility of relative enhancement by choosing appropriate kinematical constraints. In Fig.3, we display, for unpolarized scattering, some of the distributions wherein the differences are more prominent.

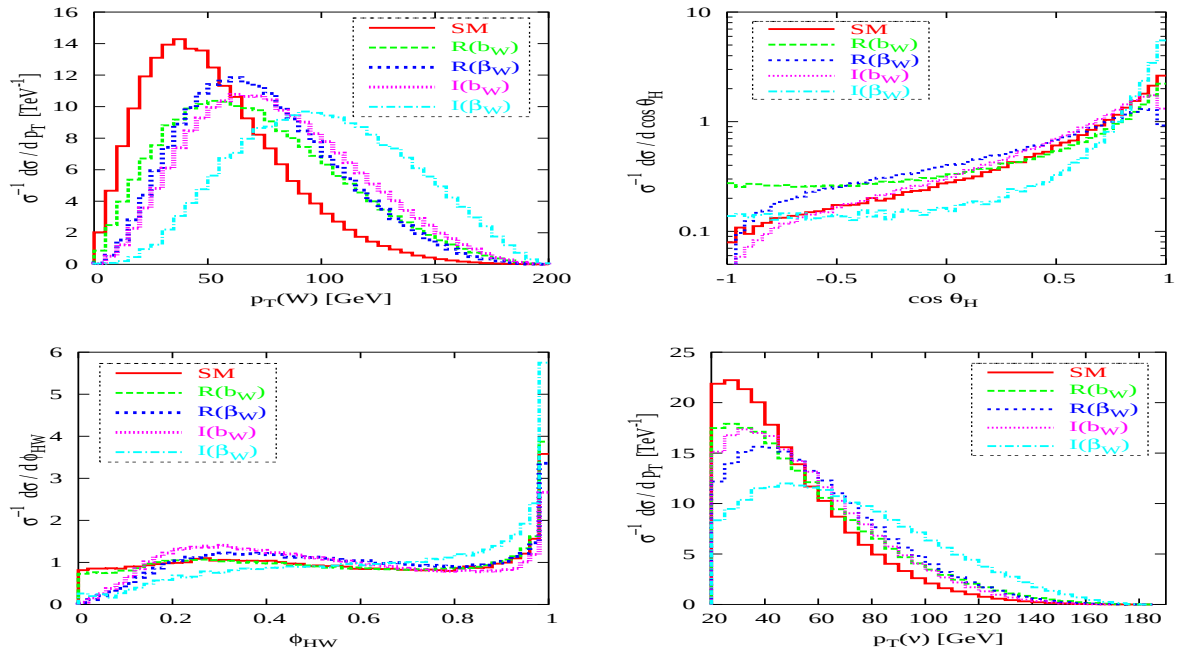

Figure 3: *Various kinematical distributions for unpolarized scattering with the acceptance cuts augmented by the requirement of* $\sin\phi_{HW} > 0$.

4 Results and Discussions

4.1 Unpolarized Beams

Although, as Fig.2 demonstrates, some of the anomalous contributions to the cross section have a strong dependence on the beam polarization, we refrain from using this at the outset, and confine ourselves to unpolarized scattering. Instead, we concentrate initially on devising appropriate phase-space restrictions so as to enhance a given contribution with respect to the SM one as also the others. Clearly, the former objective cannot be reached for the contribution proportional to Δa_W as it is identical to the SM one in all the phase-space distributions. Hence, a measurement of Δa_W has, of necessity, to be based on a counting measurement.

As has already been mentioned, the $\hat{T}$-odd couplings $\mathcal{I}(b_W)$ and $\mathcal{R}(\beta_W)$ do not contribute to the total cross section, or even to partial ones as long as the phase space is $\hat{T}$-even. This, then, constitutes a simple method of eliminating them from the analysis thereby allowing us to concentrate on the other three.

4.1.1 $\hat{T}$ even Couplings $\Delta a_W, \mathcal{R}(b_W)$ and $\mathcal{I}(\beta_W)$

As a perusal of Fig.3 shows, the differential distributions for the Δa_W and $\mathcal{R}(b_W)$ contributions are not very dissimilar and, hence, it is difficult to separate these two effects. The relative contribution of $\mathcal{I}(\beta_W)$, on the other hand, can be enhanced or reduced upon the use of different cuts on kinematic observables. A partial list of such cuts and the corresponding cross sections is displayed in Table 2.

Cut		σ_0	σ_1	σ_4
$\mathcal{C}_0$	Acceptance cuts	4.15	-16.10	-1.96
$\mathcal{C}_1$	$p_{_T}(W) \geq 80$ GeV and $\mid \sin\phi_{HW} \mid \geq 0.4$	0.25	-2.58	-0.73
$\mathcal{C}_2$	$p_{_T}(W) \geq 80$ GeV and $p_{_T}^{\rm miss} \geq 60$ GeV	0.19	-2.37	-0.74
$\mathcal{C}_3$	$p_{_T}(W) \leq 80$ GeV and $\mid \sin\phi_{HW} \mid \leq 0.4$	1.11	-2.55	0.18
$\mathcal{C}_4$	$p_{_T}(W) \leq 80$ GeV and $\mid \cos\theta_{_H} \mid \leq 0.8$	1.89	-5.56	0.044
$\mathcal{C}_5$	$p_{_T}(W) \geq 80$ GeV and $\mid \sin\phi_{HW} \mid \leq 0.4$	0.50	-3.49	-0.62

Table 2: *Various cuts and the corresponding rates, in femtobarns, for unpolarized scattering with* $\sqrt{s_{ee}} = 500$ *GeV.*

The set of cuts $\mathcal{C}_3$, and even more convincingly, $\mathcal{C}_4$, eliminates the bulk of the $\mathcal{I}(\beta_W)$ contribution. Assuming, for the moment, that the anomalous couplings are of the same order, the imposition of such cuts would allow us to neglect the presence of even a non-zero $\mathcal{I}(\beta_W)$ and instead impose a constraint on particular combinations of Δa_W and $\mathcal{R}(b_W)$.

For example, with the use of cut $\mathcal{C}_3$, the rate depends on the combination

$$\eta_3 = 2\,\Delta a_W - 2.30\,\mathcal{R}(b_W) \quad , \text{viz} \quad \sigma(\mathcal{C}_3) \approx \sigma_0\,(1+\eta_3) = 1.11\,(1+\eta_3) \tag{13}$$

and, thus, for an integrated luminosity of 500 fb^{-1}, the lack of a deviation from the SM expectation values would give us a $3\,\sigma$ limit on η_3, namely

$$|\,\eta_3\,| \leq\ 0.13\ . \tag{14}$$

Similarly, the use of $\mathcal{C}_4$ results in

$$\sigma(\mathcal{C}_4) = \sigma_0\,(1+\eta_4) = 1.89\,(1+\eta_4)\,, \text{with} \qquad \eta_4 = 2\,\Delta a_W - 2.94\,\mathcal{R}(b_W). \tag{15}$$

This results in $3\,\sigma$ bound on η_4 of

$$|\,\eta_4\,| \leq\ 0.10. \tag{16}$$

Contrary to $\mathcal{C}_{3,4}$, the cuts $\mathcal{C}_{1,2}$ serve to enhance the effect of $\mathcal{I}(\beta_W)$, though not to the extent that the effects of the other two may be entirely neglected. Consequently, we can constrain only certain linear combinations of the three, viz.

$$\begin{array}{rcll} |\ 2\,\Delta a_W - 10.36\,\mathcal{R}(b_W) - 2.93\,\mathcal{I}(\beta_W)\,| & \leq & 0.27 & (\text{using cut}\ \ \mathcal{C}_1) \\ |\ 2\,\Delta a_W - 12.25\,\mathcal{R}(b_W) - 3.84\,\mathcal{I}(\beta_W)\,| & \leq & 0.30 & (\text{using cut}\ \ \mathcal{C}_2). \end{array} \tag{17}$$

If we make the simplifying assumption that only one anomalous coupling may be non-zero, the corresponding limits are easy to obtain. The strongest such limits are listed in Table 3.

Coupling	3σ bound	Observable Used
$\lvert\,\Delta a_W\,\rvert$	0.050	σ with $\mathcal{C}_4$
$\lvert\,\mathcal{R}(b_W)\,\rvert$	0.035	σ with $\mathcal{C}_4$
$\lvert\,\mathcal{I}(\beta_W)\,\rvert$	0.078	σ with $\mathcal{C}_2$

Table 3: *Achievable upper limits (3σ) on Δa_W, $\mathcal{R}(b_W)$ and $\mathcal{I}(\beta_W)$, under the assumption that only one of the couplings is non-zero. An integrated luminosity of* 500 fb^{-1} *using unpolarized beams has been assumed.*

While individual limits might be strong and interesting in their own right, it is of importance to investigate how well the couplings may be resolved. A simple way would be to consider two of the couplings at a time (assuming the third to be vanishing) and impose different constraints on such a plane. As we are working in the linear approximation, all such constraints, for a given observable, would naturally result in an infinite linear strip as the allowed region. The intersection of such strips for mutually exclusive observables would, then, constitute the region of interest. In Fig.4, we display this for each of the three combinations of anomalous couplings. A more general analysis keeping all the three couplings non-zero is possible, and quite straightforward. Demanding that, for a combination of such couplings to be allowed, the observables corresponding to each of

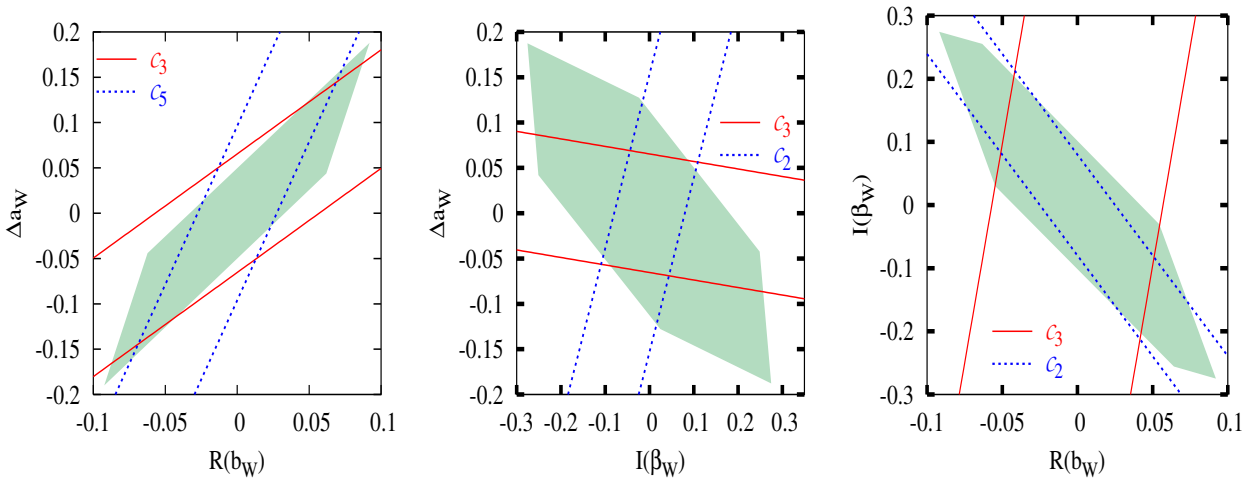

Figure 4: *The pairs of oblique lines denote the region allowed by the corresponding cut, at the* $3\,\sigma$ *level, when the third anomalous coupling is identically zero. Intersection of strips, thus, gives the area allowed by both the observables. The shaded regions constitute the projections of the parameter space that leads to observables indistinguishable from the SM expectations for each of the cuts of Table 2 when all three couplings are allowed to be non-zero. In each case, an integrated luminosity of 500* fb^{-1} *has been used.*

the cuts of Table 2 must be indistinguishable from the SM expectations, we generate a three-dimensional volume of the allowed parameter space. In Fig.4, we project such a 3σ volume onto the three different planes. It is reassuring to note that a non-zero value of $\mathcal{I}(\beta_W)$ has relatively little role to play in the constraints in the Δa_W–$\mathcal{R}(b_W)$ plane, thereby vindicating our intermediate approximation of neglecting this contribution. This, of course, is just a consequence of the smallness of the $\mathcal{I}(\beta_W)$ contribution once $\mathcal{C}_3$ is imposed. Analogous features are displayed by the projections on the Δa_W–$\mathcal{I}(\beta_W)$ and $\mathcal{R}(b_W)$–$\mathcal{I}(\beta_W)$ planes as well. The simultaneous limits obtained from these shaded regions of Fig. 4 are given in Table 4.

Coupling	$3\,\sigma$ bound
$\mid \Delta a_W \mid$	0.19
$\mid \mathcal{R}(b_W) \mid$	0.092
$\mid \mathcal{I}(\beta_W) \mid$	0.27

Table 4: *Simultaneous limits on anomalous couplings at* 3σ *level, based on shaded regions of Fig. 4, using unpolarized beams for an integrated luminosity of* $500\,\mathrm{fb}^{-1}$.

4.1.2 $\hat{T}$ odd Couplings $\mathcal{I}(b_W)$ and $\mathcal{R}(\beta_W)$

As already described above, the imaginary parts of b_W and β_W do not contribute to the total rate on account of being odd under naive time-reversal. However, on restricting the W-boson to lie above the plane of production of the Higgs (defined in conjunction with the beam axis), *i.e.* on requiring $\sin\phi_{HW} \geq 0$, we have, for the corresponding partial cross-section,

$$\begin{aligned} \sigma(\sin\phi_{HW} \geq 0) &= 2.07\ (1 + 2\ \Delta a_W) - 8.04\ \mathcal{R}(b_W) - 0.982\ \mathcal{I}(\beta_W) \\ &+ 1.50\ \mathcal{I}(b_W) - 3.11\ \mathcal{R}(\beta_W). \end{aligned} \tag{18}$$

For events in the other hemisphere ($\sin\phi_{HW} \leq 0$), the contributions corresponding to Δa_W, $\mathcal{R}(b_W)$ and $\mathcal{I}(\beta_W)$ (i.e. $\sigma_{0,1,4}$) remain the same, while the contributions corresponding to couplings $\mathcal{R}(\beta_W)$ and $\mathcal{I}(b_W)$ ($\sigma_{2,3}$) reverse sign. This, then, prompts the use of a $\hat{T}$-odd asymmetry of the form

$$\begin{aligned} \mathcal{A} &\equiv \frac{\sigma_{\sin\phi_{HW}\geq 0} - \sigma_{\sin\phi_{HW}\leq 0}}{\sigma_{\sin\phi_{HW}\geq 0} + \sigma_{\sin\phi_{HW}\leq 0}} \\ &= \frac{[3.0\ \mathcal{I}(b_W) - 6.22\ \mathcal{R}(\beta_W)]}{4.15\ \ [(1 + 2\ \Delta a_W) - 7.76\ \mathcal{R}(b_W) - 0.946\ \mathcal{I}(\beta_W)]}\ , \end{aligned} \tag{19}$$

with the corresponding fluctuation in the measurement being given by

$$(\delta\mathcal{A})^2 = \frac{1 - \mathcal{A}_{SM}^2}{\sigma_{SM}\ \mathcal{L}} + \frac{\epsilon^2}{2}\ (1 - \mathcal{A}_{SM}^2)^2\ . \tag{20}$$

It should be noted that the asymmetry vanishes identically within the SM. A glance at the various distributions of Fig.3 shows that the employment of further kinematic cuts do not alter the relative contributions of $\mathcal{I}(b_W)$ and $\mathcal{R}(\beta_W)$ in any significant way. Thus, with unpolarized beams, the best bounds on these two couplings are obtained from Equation 19 and, for an integrated luminosity of 500 fb^{-1}, reads

$$|\ 1.50\ \mathcal{I}(b_W) - 3.11\ \mathcal{R}(\beta_W)\ | \leq 0.14 \tag{21}$$

at the 3σ level. Note that, in deriving the above, we have neglected the anomalous contributions in the denominator of Equation(19), which is in consonance with our approximation of retaining terms which are at best linear in the anomalous couplings. Once again, if we assume that only one of these is non-zero, the corresponding 3σ bounds are

$$|\ \mathcal{I}(b_W)\ | \leq 0.092 \qquad \text{and} \qquad |\ \mathcal{R}(\beta_W)\ | \leq 0.045\ . \tag{22}$$

4.2 Polarized Beams

Having exhausted the possible ways that unpolarized $e^-\gamma$ scattering could be used to probe the WWH vertex, we now examine the role, if any, of beam polarization. Since the dependence on e^- polarization is trivial (only e_L^- contributes to the process under consideration), we choose to neglect this, while noting that having a left-polarized electron will only serve to rescale both the signal and the background in an identical fashion, thereby

improving the statistical significance. Concentrating on the non-trivial dependence of the cross section on the photon polarization, we note that the latter is a function, vide Equation (8), of the beam and laser polarizations. While the laser can be polarized fully, the beam polarization is unlikely to be much higher than 80%. We, thus, choose four different combinations, namely

$$\begin{aligned} a: &\quad (P_L, P_b) = (+1, +0.8) \\ b: &\quad (P_L, P_b) = (-1, -0.8) \\ c: &\quad (P_L, P_b) = (+1, -0.8) \\ d: &\quad (P_L, P_b) = (-1, +0.8) \end{aligned} \tag{23}$$

and associate a given mode with one-fourth of the total integrated luminosity, viz. 125fb^{-1} each. The corresponding rates, on imposition of the acceptance cuts alone are given in Table 5. As could have been easily surmised from Fig.2, of the five cross sections $\sigma_{0\ldots4}$,

(P_L, P_b)		σ_0	σ_1	σ_4
σ_{Pa}	$(+1, +0.8)$	3.26	-11.28	2.88
σ_{Pb}	$(-1, -0.8)$	3.47	-15.25	-6.27
σ_{Pc}	$(+1, -0.8)$	5.13	-21.16	-9.97
σ_{Pd}	$(-1, +0.8)$	4.96	-16.95	5.44

Table 5: *Cross-sections for various polarization combinations with only acceptance cuts imposed.*

polarization dependence is maximal for that proportional to $\mathcal{I}(\beta_W)$ followed by that for the $\mathcal{I}(b_W)$ term. Of course, the latter contribution vanishes identically if integrated over a symmetric phase-space. As discussed before, imposition of various cuts may enhance or reduce the relative contributions of different anomalous couplings. Of the four polarization combinations of Equation (23), the first one (a) was not found to be significantly useful. The cross-sections obtained after imposing further cuts on the other three combinations of polarization are given in Table 6.

As a non-zero Δa_W results in just a rescaling of the SM cross section, the use of polarized beam naturally does not lead to any significant improvement in its determination. However, the relative contributions of $\mathcal{R}(b_W)$ and $\mathcal{I}(\beta_W)$ can be enhanced by imposing various cuts. The strongest limits are derived using the cut $\mathcal{C}_{P3}$ on σ_{Pc} ($P_T(W) \geq 75\text{GeV}$ for $(P_L, P_b) = (+1, -.8)$) which gives

$$\mid 2\ \Delta a_W - 8.67\ \mathcal{R}(b_W) - 4.73\ \mathcal{I}(\beta_W)\ \mid \leq\ 0.25. \tag{24}$$

Once again, on assumption of only one of these couplings being non-zero leads to

$$\begin{aligned} \mid \mathcal{R}(b_W) \mid &\ \leq\ 0.029 \\ \mid \mathcal{I}(\beta_W) \mid &\ \leq\ 0.053. \end{aligned} \tag{25}$$

$$\tag{26}$$

These limits should be compared to those of Table 3. It is to be noted that these, stronger, limits have been derived using an integrated luminosity of only $125\,\text{fb}^{-1}$. Since

Cut name	Cut Description
$\mathcal{C}_{P1}$	$p_T(W) \leq 75$ GeV
$\mathcal{C}_{P2}$	$p_T(W) \leq 75$ GeV and $\cos\theta_H \leq 0$
$\mathcal{C}_{P3}$	$p_T(W) \geq 75$ GeV
$\mathcal{C}_{P4}$	$p_T(W) \geq 75$ GeV and $\cos\theta_W \geq 0$

	$b : (P_L,\ P_b) = (-1,\ -.8)$			$c : (P_L,\ P_b) = (+1,\ -.8)$			$d : (P_L,\ P_b) = (-1,\ +.8)$		
cut	σ_0	σ_1	σ_4	σ_0	σ_1	σ_4	σ_0	σ_1	σ_4
$\mathcal{C}_{P1}$	2.75	-8.8	-3.16	3.91	-11.23	-4.31	3.85	-10.27	3.23
$\mathcal{C}_{P2}$	0.41	-2.21	-0.10						
$\mathcal{C}_{P3}$	0.72	-6.47	-3.10	1.20	-10.40	-5.68	1.09	-6.67	2.20
$\mathcal{C}_{P4}$	0.08	-1.83	-0.87						

Table 6: *The description of cuts over and above acceptance cuts for the study with polarized beams and the corresponding cross-sections (in femtobarns).*

the couplings cannot be isolated, we should be looking at the simultaneous limits which are to be obtained from the graphs (following the way it was done in section 4.1.1 for the unpolarized case). It should be noted from Table 5 that the contribution of $\mathcal{I}(\beta_W)$ has very strong dependence on the value of $(P_L,\ P_b)$. This fact is exploited to obtain constraints in the $\Delta a_W - \mathcal{I}(\beta_W)$ and $\mathcal{R}(b_W) - \mathcal{I}(\beta_W)$ planes. These simultaneous constraints are shown in Fig. 5 and the limits obtained are listed in Table 9. It should be noted that the combination (a) of polarization *i.e.* $(P_L, P_b) = (+1, +0.8)$ is not a very sensitive probe and hence it has been disregarded in obtaining these simultaneous limits.

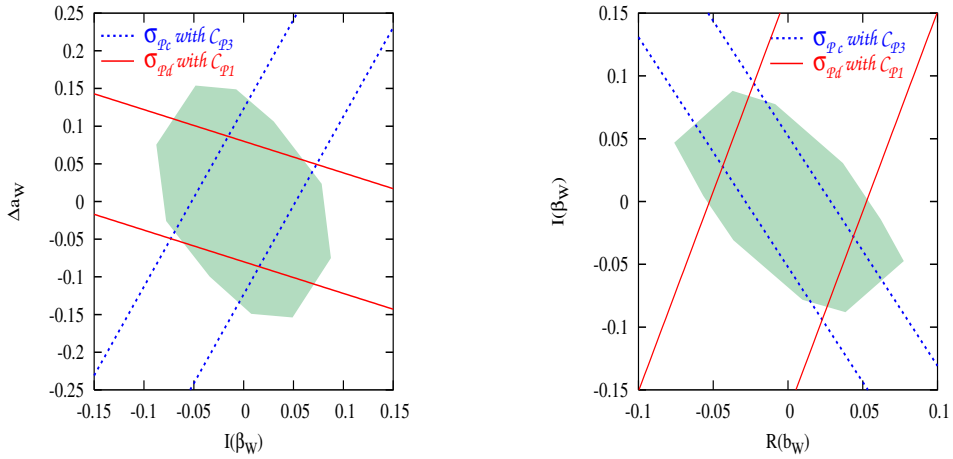

Figure 5: *The allowed regions in the $\mathcal{I}(\beta_W) - \Delta a_W$ and $\mathcal{R}(b_W) - \mathcal{I}(\beta_W)$ planes. The shaded regions constitute the projections of the parameter space that leads to observables indistinguishable, at the $3\,\sigma$ level, from the SM expectations for each of the cuts given in Table 6 and an integrated luminosity of $125\,\text{fb}^{-1}$. The pairs of oblique lines denote the region allowed by the corresponding cut when the third anomalous coupling is identically zero.*

As before, to get contribution from the $\hat{T}$-odd couplings $\mathcal{I}(b_W)$ and $\mathcal{R}(\beta_W)$, we have to restrict ourselves to only half of the phase space, namely, $\sin\phi_{HW} \geq 0$. These partial cross-sections for various polarizations are given in Table 7.

We construct the $\hat{T}$-odd asymmetry $\mathcal{A}$ as before and find that the best limits are obtained for the case (d), namely $(P_L, Pb) = (-1, +0.8)$. For this case,

$$\mathcal{A} = \mathcal{A}_d = \frac{0.99\,\mathcal{I}(b_W) - 3.22\,\mathcal{R}(\beta_W)}{2.48\,[(1 + 2\,\Delta a_W) - 3.42\,\mathcal{R}(b_W) + 1.09\,\mathcal{I}(\beta_W)]}\,. \tag{27}$$

Using the cross-section for this case with only acceptance cuts, namely σ_{Pd} from Table 7, we obtain

$$|\ 2\,\Delta a_W - 3.42\,\mathcal{R}(b_W) + 1.09\,\mathcal{I}(\beta_W)\ | \leq 0.12. \tag{28}$$

Using Equation 28 and Equation 27, the 3σ bound on the asymmetry gives us

$$|\ 0.99\,\mathcal{I}(b_W) - 3.22\,\mathcal{R}(\beta_W)\ | \leq 0.14. \tag{29}$$

Keeping only one of these to be non-zero, we obtain the following individual limits on them at 3σ:

$$|\ \mathcal{I}(b_W)\ | \leq 0.15 \qquad \text{and} \qquad |\ \mathcal{R}(\beta_W)\ | \leq 0.047 \tag{30}$$

for an integrated luminosity of 125 fb^{-1}. Comparing with Equation 22, we observe that the individual limits are not improved by use of polarized photon beam. This is because of reduction in luminosity. However, using any pair of rates in Table 7, it is possible to obtain the allowed region in $\mathcal{I}(b_W) - \mathcal{R}(\beta_W)$ plane which can be used to put the simultaneous limits on these couplings. This was not possible with the unpolarized photons. The constraints in $\mathcal{I}(b_W) - \mathcal{R}(\beta_W)$ plane using σ_{Pc} and σ_{Pd} of Table 7 are given in Fig. 6. Since the intersecting region given by two oblique lines and the shaded regions are same, it is clear that the cases a and d (*i.e.* $(P_L, P_b) = (+1,\ +0.8)$ and $(P_L, P_b) = (-1,\ -0.8)$) do not play any role in isolating these two couplings. We summarise in Table 8, the individual limits on various anomalous couplings and in Table 9 the simultaneous limits.

It should be noted that the simultaneous limits obtained are much better compared to those obtained with unpolarized beams. This is particularly apparent for the case of $\mathcal{I}(\beta_W)$. Also we are able to obtain the simultaneous limits for $\mathcal{I}(b_W)$ and $\mathcal{R}(\beta_W)$.

5 Use of the $e^+\,\gamma$ initial state

Until now, in constructing observables, we have exploited only the transformation of the operators of Equation 2 under either P or $\hat{T}$. We now consider the action of the composite

(P_L, P_b)		σ_0	σ_1	σ_4	σ_3	σ_2
σ_{Pa}	$(+1, +0.8)$	1.63	-5.64	1.44	0.74	-2.03
σ_{Pb}	$(-1, -0.8)$	1.74	-7.63	-3.12	1.75	-2.94
σ_{Pc}	$(+1, -0.8)$	2.56	-10.82	-4.98	2.59	-4.43
σ_{Pd}	$(-1, +0.8)$	2.48	-8.48	2.71	0.99	-3.22

Table 7: *Cross-sections for polarized beams with acceptance cuts and with* $\sin\phi_{HW} \geq 0$.

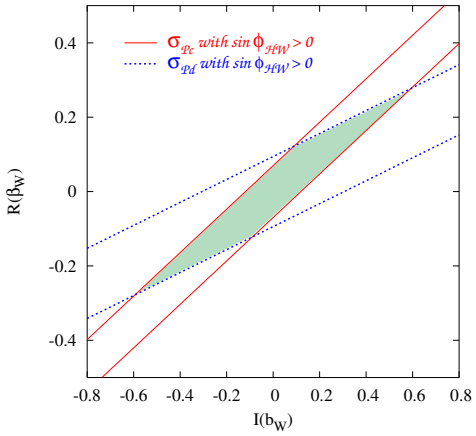

Figure 6: *The region in the $\mathcal{I}(b_W) - \mathcal{R}(\beta_W)$ plane consistent with 3σ variations in the assymetries with polarized photon beams for an integrated luminosity of 125 fb^{-1} per polarization combination. The pair of oblique lines correspond to σ_{Pc} and σ_{Pd} with $\sin\phi_{HW} \geq 0$ while the shaded region is obtained by demanding that the anomalous events can't be distinguished from SM values at 3σ corresponding to all combinations of (P_L, P_b) given in Table 7.*

Coupling	3 σ bound	Observable Used
$\mid \mathcal{R}(b_W) \mid$	0.029	σ_{Pc} with $\mathcal{C}_{P3}$
$\mid \mathcal{I}(\beta_W) \mid$	0.053	σ_{Pc} with $\mathcal{C}_{P3}$
$\mid \mathcal{I}(b_W) \mid$	0.150	$\mathcal{A}_d$
$\mid \mathcal{R}(\beta_W) \mid$	0.047	$\mathcal{A}_d$

Table 8: *Individual Limits on anomalous couplings at 3σ level using polarized beams at an integrated luminosity of* $125\,\mathrm{fb}^{-1}$.

Coupling	3 σ bound	Graph Used
$\mid \Delta a_W \mid$	0.150	Fig. 5
$\mid \mathcal{R}(b_W) \mid$	0.078	Fig. 5
$\mid \mathcal{I}(\beta_W) \mid$	0.088	Fig. 5
$\mid \mathcal{I}(b_W) \mid$	0.58	Fig. 6
$\mid \mathcal{R}(\beta_W) \mid$	0.27	Fig. 6

Table 9: *Simultaneous Limits on anomalous couplings at 3σ level using polarized beams at an integrated luminosity of* $125\,\mathrm{fb}^{-1}$.

discrete symmetry $P\hat{T}$. This is best achieved by comparing the results obtained until now using the $e^-\,\gamma$ colliders with those expected from the conjugate process, namely

$$e^+\,\gamma \longrightarrow \bar{\nu}\,W^+\,H$$

5.1 Unpolarized Beams

The total cross-section for the conjugate process is related to that obtained earlier in a simple fashion:

$$\begin{aligned}\sigma_{e^+\gamma} &= [\ \sigma_0\ (1+2\ \Delta a_W) + \sigma_1\ \mathcal{R}(b_W) + \sigma_2\ \mathcal{R}(\beta_W)]_{e^-\gamma} \\ &\quad - [\sigma_3\ \mathcal{I}(b_W) + \sigma_3\ \mathcal{I}(b_W)]_{e^-\gamma}\,. \end{aligned} \tag{31}$$

This leads us to construct the asymmetry

$$\begin{aligned}\mathcal{A}_{C1_{\rm unpol}} &\equiv \frac{\sigma_{e^+\gamma} - \sigma_{e^-\gamma}}{\sigma_{e^+\gamma} + \sigma_{e^-\gamma}} \\ &= \frac{2\ [\sigma_3\ \mathcal{I}(b_W) + \sigma_4\ \mathcal{I}(\beta_W)]_{e^+\gamma}}{2\ [\sigma_0\ (1+2\ \Delta a_W) + \sigma_1\ \mathcal{R}(b_W) + \sigma_2\ \mathcal{R}(\beta_W)]_{e^+\gamma}} \\ &\simeq \frac{1}{\sigma_0}\,[\sigma_3\ \mathcal{I}(b_W) + \sigma_4\ \mathcal{I}(\beta_W)]_{e^+\gamma}\,, \end{aligned} \tag{32}$$

where the approximate equality follows from our premise of retaining only terms linear in the anomalous couplings. If no cut is imposed on $\sin\phi_{HW}$, the numerator contains only the $\mathcal{I}(\beta_W)$ term allowing us to obtain a direct bound on his coupling alone, something that we were hitherto unable to. With only the acceptance cuts imposed, we obtain for the 3σ bound

$$|\ \mathcal{I}(\beta_W)\ | \leq\ 0.14, \tag{33}$$

using an integrated luminosity of 250 fb^{-1} for each of $e^-\,\gamma$ and $e^+\,\gamma$ modes. As was shown in section 4.1.1, imposing further cut of $p_{_T}(W) \geq 80$ GeV and $|\ \sin\phi_{HW}\ | \geq\ 0.4$ (the cut $\mathcal{C}_1$ of Table 2), enhances the relative effect of $\mathcal{I}(\beta_W)$. With this set of cuts imposed, we get, instead

$$|\ \mathcal{I}(\beta_W)\ | \leq 0.092 \tag{34}$$

irrespective of the value of $\mathcal{R}(\beta_W)$ or Δa_W.

We may also use the $e^+\,\gamma$ mode to resolve between $\mathcal{R}(\beta_W)$ and $\mathcal{I}(b_W)$, which we have been unable to working with the $e^-\,\gamma$ mode alone. As we have already seen (Equation 19), an asymmetry constructed out of the azimuthal separation between the H and the W would, in general, pick up the contributions proportional to $\mathcal{R}(\beta_W)$ and $\mathcal{I}(b_W)$. Read in conjunction with Equation 32, we have, for a new asymmetry,

$$\begin{aligned}\mathcal{A}_{C2_{\rm unpol}} &= \frac{(\sigma_{++} - \sigma_{+-}) - (\sigma_{-+} - \sigma_{--})}{(\sigma_{++} + \sigma_{+-}) + (\sigma_{-+} + \sigma_{--})} \\ &= \frac{-4\ [\sigma_3\ \mathcal{I}(b_W)]_{e^-\gamma,\ \sin\phi_{HW}>0}}{4\ [\sigma_0\ (1+2\ \Delta a_W) + \sigma_1\ \mathcal{R}(b_W)]_{e^-\gamma,\ \sin\phi_{HW}>0}} \\ &\simeq -\mathcal{I}(b_W)\ \left[\frac{\sigma_3}{\sigma_0}\right]_{e^-\gamma,\ \sin\phi_{HW}>0}., \end{aligned} \tag{35}$$

where

$$\begin{aligned}\sigma_{++} &= \sigma_{e^+\gamma,\ \sin\phi_{HW}>0} \\ \sigma_{+-} &= \sigma_{e^+\gamma,\ \sin\phi_{HW}<0} \\ \sigma_{-+} &= \sigma_{e^-\gamma,\ \sin\phi_{HW}>0} \\ \sigma_{--} &= \sigma_{e^-\gamma,\ \sin\phi_{HW}<0} \end{aligned} \tag{36}$$

Use of this asymmetry gives, for the 3σ bound,

$$| \mathcal{I}(b_W) | \leq 0.096 \tag{37}$$

for an integrated luminosity of 250 fb^{-1} per mode.

And finally to isolate $\mathcal{R}(\beta_W)$, we may construct yet another asymmetry

$$\begin{aligned}
\mathcal{A}_{C3_{\rm unpol}} &= \frac{(\sigma_{++} - \sigma_{--}) - (\sigma_{+-} - \sigma_{-+})}{(\sigma_{++} + \sigma_{--}) + (\sigma_{+-} + \sigma_{-+})} \\
&= \frac{4\ [\sigma_2\ \mathcal{R}(\beta_W)]_{e^+\gamma,\ \sin\phi_{HW}>0}}{4\ [\sigma_0\ (1 + 2\ \Delta a_W) + \sigma_1\ \mathcal{R}(b_W)]_{e^-\gamma,\ \sin\phi_{HW}>0}} \\
&\simeq -\mathcal{R}(\beta_W)\ \left[\frac{\sigma_4}{\sigma_0}\right]_{e^+\gamma,\ \sin\phi_{HW}>0}.
\end{aligned} \tag{38}$$

Thus for the 3σ bound on $| \mathcal{R}(\beta_W) |$, we get

$$| \mathcal{R}(\beta_W) | \leq 0.046 \tag{39}$$

using an integrated luminosity of 250 fb^{-1} per mode.

5.2 Polarized Beams

It is easy to see that the introduction of non-zero beam polarization would lead to a relation between $e^-\gamma$ and $e^+\gamma$ cross-sections that is analogous to that of Equation 31, namely

$$\begin{aligned}
\sigma_{e^+\gamma,(P_L,P_b)} &= [(1 + 2\ \Delta a_W)\ \sigma_0 + \mathcal{R}(b_W)\sigma_1 + \mathcal{R}(\beta_W)\sigma_2]_{e^-\gamma\ ,(-P_L,-P_b)} \\
&\quad - [\mathcal{I}(\beta_W)\sigma_4 + \mathcal{I}(b_W)\sigma_3]_{e^-\gamma\ ,(-P_L,-P_b)}
\end{aligned} \tag{40}$$

This is easy to understand since reversing both P_L and P_b results in reversing the photon polarization while preserving the density distribution (see Equation 8) We construct asymmetries to take advantage of these. The best limits are obtained from

$$\begin{aligned}
\mathcal{A}_{C1_{\rm pol}} &\equiv \frac{\sigma_{e^-\gamma(+1,-0.8)} - \sigma_{e^+\gamma(-1,+0.8)}}{\sigma_{e^-\gamma(+1,-0.8)} + \sigma_{e^+\gamma(+1,-0.8)}} \\
&= \frac{2\ [\mathcal{I}(\beta_W)\,\sigma_4 + \mathcal{I}(b_W)\,\sigma_3\ ]_{e^-\gamma,(+1,-0.8)}}{2\ [(1 + 2\ \Delta a_W)\,\sigma_0 + \mathcal{R}(b_W)\,\sigma_1 + \mathcal{R}(\beta_W)\sigma_2]_{e^-\gamma,(+1,-0.8)}} \\
&\simeq \left[\frac{\mathcal{I}(\beta_W)\ \sigma_2 + \mathcal{I}(b_W)\ \sigma_3}{\sigma_0}\right]_{e^-\gamma,(+1,-0.8)}.
\end{aligned} \tag{41}$$

With only acceptance cuts imposed, $\mathcal{I}(b_W)$ does not contribute to the total cross-section and thus above asymmetry depends only on $\mathcal{I}(\beta_W)$. We obtain for the 3σ bound

$$| \mathcal{I}(\beta_W) | \leq 0.044 \tag{42}$$

using integrated luminosity of 125 fb^{-1} per polarization combination. This limit is stronger than the one obtained using unpolarized photons (Equation 33).

Coupling	3 $\delta\mathcal{A}$ bound	Observable Used	Luminosity (in fb^{-1})
$\mid \mathcal{I}(\beta_W) \mid$	0.092	$\mathcal{A}_{C1_{\rm unpol}}$ with $\mathcal{C}_1$	250
$\mid \mathcal{I}(\beta_W) \mid$	0.044	$\mathcal{A}_{C1_{\rm pol}}$ with acceptance cuts	125
$\mid \mathcal{I}(b_W) \mid$	0.096	$\mathcal{A}_{C3_{\rm unpol}}$ with acceptance cuts	250
$\mid \mathcal{I}(b_W) \mid$	0.220	$\mathcal{A}_{C3_{\rm pol}}$ with acceptance cuts	125
$\mid \mathcal{R}(\beta_W) \mid$	0.046	$\mathcal{A}_{C2_{\rm unpol}}$ with acceptance cuts	250
$\mid \mathcal{R}(\beta_W) \mid$	0.068	$\mathcal{A}_{C2_{\rm pol}}$ with acceptance cuts	125

Table 10: *Comparison of limits on anomalous couplings at 3σ level using unpolarized and polarized beams.*

The other two couplings $\mathcal{I}(b_W)$ and $\mathcal{R}(\beta_W)$ can be also isolated and constrained using the mixed asymmetries as before. To get limits on $\mathcal{I}(b_W)$, we construct the following asymmetry

$$\begin{aligned}
\mathcal{A}_{C2_{\rm pol}} &\equiv \frac{\left[\sigma_{\sin\phi>0} - \sigma_{\sin\phi<0}\right]_{e^+\gamma,(+1,-0.8)} - \left[\sigma_{\sin\phi>0} - \sigma_{\sin\phi<0}\right]_{e^-\gamma,(-1,+0.8)}}{\left[\sigma_{\sin\phi>0} + \sigma_{\sin\phi<0}\right]_{e^+\gamma,(+1,-0.8)} + \left[\sigma_{\sin\phi>0} + \sigma_{\sin\phi<0}\right]_{e^-\gamma,(-1,+0.8)}} \\
&= \left[\frac{4\,\mathcal{I}(b_W)\,\sigma_3}{4\,\sigma_0\,(1+2\,\Delta a_W) + \sigma_1\,\mathcal{R}(b_W)}\right]_{e^+\gamma,\,\sin\phi>0,\,(+1,-0.8)} \\
&\simeq \mathcal{I}(b_W)\,\left[\frac{\sigma_3}{\sigma_0}\right]_{e^+\gamma,\,\sin\phi>0,\,(+1,-0.8)} \qquad (43)
\end{aligned}$$

which gives for the 3σ bound

$$\mid \mathcal{I}(b_W) \mid \leq\ 0.22 \qquad (44)$$

using integrated luminosity of 125 fb^{-1} for each of the polarization combinations.

To isolate $\mathcal{R}(\beta_W)$, we construct,

$$\begin{aligned}
\mathcal{A}_{C3_{\rm pol}} &\equiv \frac{\left[\sigma_{\sin\phi>0} - \sigma_{\sin\phi<0}\right]_{e^+\gamma,\,(+1,-0.8)} + \left[\sigma_{\sin\phi>0} - \sigma_{\sin\phi<0}\right]_{e^-\gamma,\,(-1,+0.8)}}{\left[\sigma_{\sin\phi>0} + \sigma_{\sin\phi<0}\right]_{e^+\gamma,\,(+1,-0.8)} + \left[\sigma_{\sin\phi>0} + \sigma_{\sin\phi<0}\right]_{e^-\gamma,\,(-1,+0.8)}} \\
&= \left[\frac{4\,\mathcal{R}(\beta_W)\,\sigma_2}{4\,\sigma_0\,(1+2\,\Delta a_W) + \sigma_1\,\mathcal{R}(b_W)}\right]_{e^+\gamma,\,\sin\phi>0,\,(+1,-0.8)} \\
&\simeq \mathcal{R}(\beta_W)\,\left[\frac{\sigma_4}{\sigma_0}\right]_{e^+\gamma,\,\sin\phi>0,\,(+1,-0.8)} \qquad (45)
\end{aligned}$$

which gives for the 3σ bound

$$\mid \mathcal{R}(\beta_W) \mid \leq\ 0.068 \qquad (46)$$

on using integrated luminosity of 125 fb^{-1} per polarization case.

The comparison of limits on these couplings with the ones obtained using unpolarized photons is done in the Table 10. It may be noted that the polarized photons help to improve the constraints on $\mathcal{I}(\beta_W)$ significantly over the unpolarized photons. For the other two couplings, however, the limits in fact worsen. This is due to reduction in the luminosity.

6 Conclusions

Since the WWH couplings are not contaminated by the ZZH couplings in the process studied hence $e\ \gamma$ colliders can be used to constrain the anomalous WWH couplings independent of the ZZH couplings. Thus $e\ \gamma$ colliders are better equipped than $e^+\ e^-$ colliders to study these couplings.

Comparing our results to those of Ref. [9], we find that we obtain better individual limits for all couplings, bar Δa_W, using unpolarized photon beams. These limits on $\mathcal{R}(b_W), \mathcal{I}(\beta_W)$ and $\mathcal{R}(\beta_W)$ become stronger with the use of polarized photons. Polarized photons can be also used to derive constraints on the $\mathcal{I}(b_W) - \mathcal{R}(\beta_W)$ plane, something not possible with the use of unpolarized photons. Furthermore, in Ref. [9], the authors were unable to construct observables that depend on only one of the couplings. Hence their limits on WWH couplings are not independent of each other. However, using the process $e^-\ \gamma \longrightarrow \nu\ W^-\ H$ in conjunction with the conjugate process $e^+\ \gamma \longrightarrow \bar{\nu}\ W^+\ H$, and using the $P\ \hat{T}$ properties of various contributions to the total rate, we are able to construct observables that are function of only one of the couplings. Thus we are able to derive constraints on each of the couplings $\mathcal{I}(\beta_W)$, $\mathcal{I}(b_W)$ and $\mathcal{R}(\beta_W)$ independent of the value of any other coupling. Δa_W and $\mathcal{R}(b_W)$, however, cannot be constrained independent of each other.

We also conclude that once both $e^-\ \gamma$ and $e^+\ \gamma$ initial states can be used, beam polarization does not give any significant advantage and strong limits may be obtained with the use of unpolarized photons alone.

Acknowledgment

One of us (Mamta) wants to thank Department of Science and Technology, New Delhi for providing partial support during the course of this work under the grant no. SP/S2/K-20/99.

References

[1] ALEPH, DELPHI, L3 and OPAL Collaborations, The LEP Working Group for Higgs Boson Searches, Phys. Lett. **B565**, 61 (2003);
see also http://lephiggs.web.cern.ch/LEPHIGGS/

[2] LEP Electroweak Working Group, http://lepewwg.web.cern.ch/LEPEWWG/

[3] R. Akers *et al.* [OPAL Collaboration], Z. Phys. **C61**, 19 (1994); D. Buskulic *et al.* [ALEPH Collaboration], Z. Phys. **C62**, 539 (1994); M. Acciarri *et al.* [L3 Collaboration], Z. Phys. **C62**, 551 (1994); P. Abreu *et al.* [DELPHI Collaboration], Z. Phys. **C67**, 69 (1995); D. Antreasyan *et al.* [Crystal Ball Collaboration], Phys. Lett. **B251**, 204 (1990); P. Franzini *et al.*, Phys. Rev. **D35**, 2883 (1987); J. Kalinowski and M. Krawczyk, Phys. Lett. **B361**, 66 (1995) [arXiv:hep-ph/9506291]; D. Choudhury and M. Krawczyk, Phys. Rev. **D55**, 2774 (1997) [arXiv:hep-ph/9607271].

[4] M. Carena, J. R. Ellis, A. Pilaftsis and C. E. M. Wagner, Nucl. Phys. **B586**, 92 (2000); A. Mendez and A. Pomarol, Phys. Lett. **B279**, 98 (1992); J. F. Gunion, H. E. Haber and J. Wudka, Phys. Rev. **D43**, 904 (1991); J. F. Gunion, B. Grzadkowski, H. E. Haber and J. Kalinowski, Phys. Rev. Lett. **79**, 982 (1997) [hep-ph/9704410]; I. F. Ginzburg, M. Krawczyk and P. Osland, hep-ph/0211371.

[5] G. Abbiendi *et al.* [OPAL Collaboration], Eur. Phys. J. **C37**, 49 (2004); ALEPH, DELPHI, L3 and OPAL Collaborations, The LEP Working Group for Higgs Boson Searches, LHWG-Note 2004-01.

[6] See for example, J. R. Forshaw, Pramana **63**, 1119 (2004) and discussion therein; see also D. Choudhury, T. M. P. Tait and C. E. M. Wagner, Phys. Rev. **D65**, 053002 (2002) [arXiv:hep-ph/0109097].

[7] ATLAS Collaboration, *Detector and Physics Performance Technical Design Report*, CERN-LHCC-99-14 & 15 (1999); CMS Collaboration, *Technical Design Report*, CERN-LHCC-97-10 (1997).

[8] R. L. Kelly and T. Shimada, Phys. Rev. **D23**, 1940 (1981); P. Kalyniak, J. N. Ng and P. Zakarauskas, Phys. Rev. **D29**, 502 (1984). W. Kilian, M. Kramer and P. M. Zerwas, Phys. Lett. **B373**, 135 (1996) [arXiv:hep-ph/9512355].

[9] S.S. Biswal, D. Choudhury, R.M. Godbole and R.K. Singh, Phys.Rev.**D73**, 035001 (2006) [arXiv: hep-ph/0509070].

[10] J. C. Romao and A. Barroso, Phys. Lett. **B185**, 195 (1987).

[11] R. Rattazzi, Z. Phys. **C40**, 605 (1988).

[12] K. Hagiwara and M. L. Stong, Z. Phys. **C62**, 99 (1994).

[13] H. J. He, Y. P. Kuang, C. P. Yuan and B. Zhang, Phys. Lett. **B554**, 64 (2003) [arXiv:hep-ph/0211229].

[14] K. Hagiwara, S. Ishihara, R. Szalapski and D. Zeppenfeld, Phys. Rev. **D48**, 2182 (1993); K. Hagiwara, R. Szalapski and D. Zeppenfeld, Phys. Lett. **B318**, 155 (1993) [arXiv:hep-ph/9308347].

[15] G. J. Gounaris, F. M. Renard and N. D. Vlachos, Nucl. Phys. **B459**, 51 (1996) [arXiv:hep-ph/9509316].

[16] S. M. Lietti, A. A. Natale, C. G. Roldao, R. Rosenfeld, Phys. Lett **B97**, 243 (2001).

[17] T. Plehn, D. Rainwater and D. Zeppenfeld, Phys. Rev. Lett. **88** 051801 (2002).

[18] Bin Zhang, Yu-Ping Kuang, Hong-Jian He and C.-P. Yuan, Phys. Rev. **D67**, 114024 (2003) [arXiv:hep-ph/0303048].

[19] K. Hagiwara, S. Ishihara, J. Kamoshita and B. A. Kniehl, Eur. Phys. J. **C14**, 457 (2000) [arXiv:hep-ph/0002043].

[20] D. Atwood and A. Soni, Phys. Rev. **D45**, 2405 (1992).

[21] T. Han and J. Jiang, Phys. Rev. **D63**, 096007 (2001).

[22] P. Niezurawski, A. F. Zarnecki and M. Krawczyk, Acta Phys. Polon. **B36**, 833 (2005) [arXiv:hep-ph/0410291].

[23] Tao Han, Yu-Ping Kuang and Bin Zhang, Phys. Rev **D73**, 055010 (2006).

[24] I. F. Ginzburg, G. L. Kotkin, V. .G. Serbo and V. I. Telnov, Nucl. Instr. Meth. **205**, 47 (1983).

[25] A. Mendez and A. Pomarol, Phys. Lett. **B272**, 313 (1991).

[26] D. Choudhury, A. Datta and K. Huitu, Nucl. Phys. **B673**, 385 (2003) [arXiv:hep-ph/0302141].

[27] B. A. Kniehl, Nucl. Phys. **B352**, 1 (1991); Nucl. Phys. **B357**, 439 (1991)

[28] M. C. Gonzalez-Garcia, Int. J. Mod. Phys. **A14**, 3121 (1999) [arXiv:hep-ph/9902321]; hep-ph/9811389; V. Barger, T. Han, P. Langacker, B. McElrath and P. Zerwas, Phys. Rev. **D67**, 115001 (2003) [arXiv:hep-ph/0301097].